

---

---

# A Two-Dimensional Numerical Model which Simulates the Temperature, Salinity and Velocity Fields in Knight Inlet, British Columbia

Maureen L. Yeremy  
Royal Roads Military College<sup>1</sup>,  
Victoria, B.C., V0S 1B0.

and

Michael W. Stacey  
Department of Physics,  
Royal Military College of Canada,  
P.O. Box 17000, Kingston, Ontario, K7K 7B4.

[Original manuscript received 12 May 1997; in revised form 6 November 1997]

---

**ABSTRACT** A two-dimensional laterally integrated model of Knight Inlet, British Columbia is used to simulate the time-varying temperature, salinity and velocity fields. The model includes the influence of the wind, tides, solar heating and freshwater inflow. The level 2.5 turbulent closure scheme of Mellor and Yamada is used to parametrize the diffusion terms in the model. In this paper, two turbulent kinetic energy boundary conditions at the air-water interface are compared. One boundary condition is for an enhanced surface turbulent layer due to the flux of wind energy while the other is based on the Law of the Wall approach. The model is compared to data collected in the summer of 1989 from four moored vertical arrays. Salinity, temperature, horizontal current velocity and wind velocity were measured for about thirty days. Measurements were made throughout the water column so that the thin surface layer and deep water flows could be resolved. A moored array near the mouth of the inlet was used to provide open boundary data for the model, while the remaining data were compared to the simulated data. The modelled salinity fields were very realistic particularly when the enhanced turbulent surface layer boundary condition was used. The temperature fields were well modelled as long as the surface temperature was prescribed. The simulated velocities were very similar to those produced by a numerical model which simulated density (with the pressure effect removed) directly, instead of solving for temperature and salinity and then determining density via an equation of state.

**RÉSUMÉ** Un modèle intégré latéral à deux dimensions, à l'anse de Knight en Colombie-Britannique, a été utilisé pour simuler les champs de la température de la salinité et de la vitesse, variant dans le temps. Le modèle comprend l'influence du vent, des marées, du

---

<sup>1</sup>Now at Defence Research Establishment Ottawa, 3701 Carling Avenue, Ottawa, Ontario, K1A 0Z4.

*réchauffement solaire et du débit entrant d'eau douce. Le schéma de fermeture de turbulence au niveau 2,5 de Mellor et Yamada (1982) a été choisi pour la paramétrisation des termes de diffusion dans le modèle. Dans cet article, on a comparé deux conditions frontières de l'énergie cinétique turbulente à l'interface air-eau. Une condition frontière se réfère à une couche turbulente de surface améliorée due au flux de l'énergie éolienne, tandis que l'autre est basée sur l'approche de la loi du mur. On a comparé les données recueillies à l'été de 1989 à partir de quatre colonnes verticales captives. La salinité, la température, la vitesse du courant horizontal et la vitesse du vent ont été mesurées pendant environ trente jours. Les mesures ont été faites à travers une colonne d'eau de telle façon que la couche de la surface mince et les écoulements dans l'eau profonde pouvaient être solutionnés. Une colonne captive près de l'embouchure de l'anse a été utilisée afin de fournir des conditions limites au modèle, tandis que les autres données ont été comparées aux données simulées. Les champs de modélisation pour la salinité ont été très réalistes, particulièrement lorsqu'on emploie des conditions frontières de surface de turbulence améliorée. On a réussi à bien modéliser les champs de la température en autant que la température de surface soit disponible. Les vitesses simulées ont été très similaires à celles obtenues par un modèle numérique qui a simulé la densité (avec l'effet de la pression en moins) directement, au lieu de solutionner pour la température et la salinité et ainsi de déterminer la densité au moyen d'une équation d'état.*

---

### 1 Introduction

Knight Inlet (Figs 1 and 2) is one of many fjords found along the coastline of western Canada. The inlet has the characteristic U-shaped valley which is commonly found in fjord environments and is evidence of glacial activity from a previous Ice Age. Knight Inlet's width is relatively constant ( $\approx 3$  km) throughout its length. The inlet has an approximate length of 100 km from the mouth to the head and undergoes a significant change of direction midway along its length.

A characteristic attribute of a fjord (Embleton and King, 1968) is either a single or a series of rock basins which are interrupted by rock bars. This is observed in Knight Inlet (Fig. 3). There are two basins and two sill regions with the extreme inlet bottom depths of approximately 65 and 545 m. The inner sill is located near Hoeya Head, while the outer sill is found where the inlet intersects with the Queen Charlotte Strait.

Two glacier-fed rivers, the Franklin and Klinaklani Rivers drain from the Coast Mountain Range into this salt water inlet near its head. The majority of the fresh-water volume which flows into the inlet comes from the Klinaklani River. The added freshwater contribution from melting glaciers results in some of the greatest peak flow rates (i.e.,  $810 \text{ m}^3 \text{ s}^{-1}$ , Pickard, 1975) in the province. During the winter, because of the surrounding high elevations, most of the precipitation is in the form of snow which becomes available to the drainage system in the spring and summer seasons.

The inlet's water column is, in general, vertically stratified. The runoff which varies with the precipitation rates and seasonal temperatures, forms a brackish surface layer over the salt water estuary. This layer's thickness and distinctness are

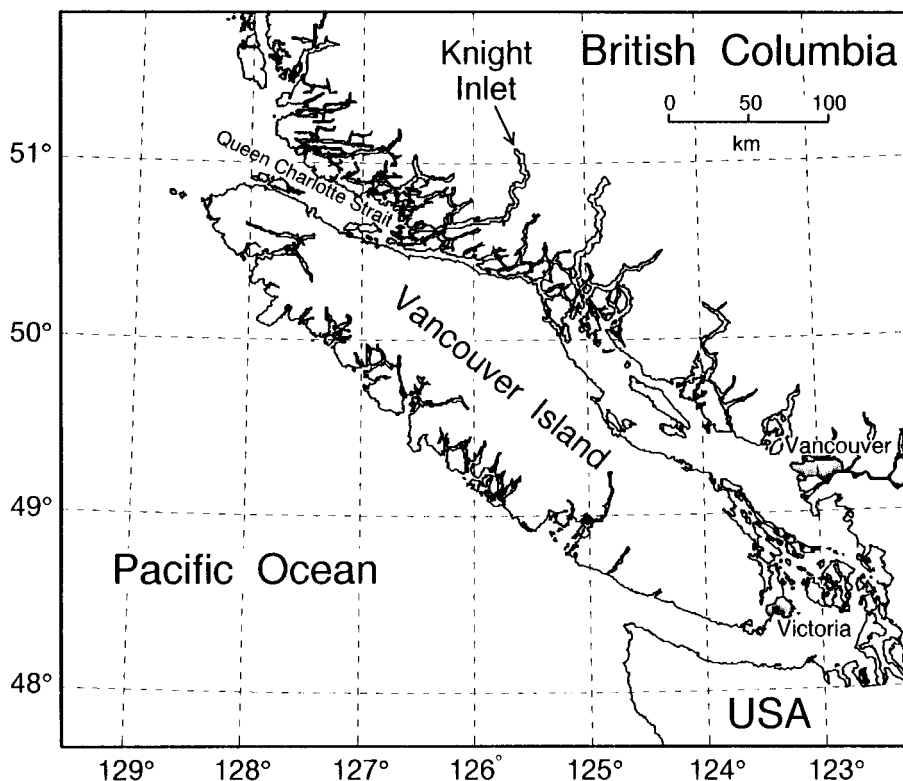


Fig. 1 Southern coastline of British Columbia showing the location of Knight Inlet.

related to factors such as runoff volume and wind (e.g., Baker and Pond, 1995). In the summer, due to the freshet, the surface layer is very distinct and has a thickness of 5–10 m. When a distinct surface layer exists, there is a classical estuarine circulation with an outflow of surface and entrained water which is compensated for by an inflow of water at depth in order to conserve salt and volume. However, the detailed circulation patterns are much more complex and are influenced by runoff, tidal and wind forcing (e.g., Baker and Pond, 1995; Stacey et al., 1995).

Energy from the barotropic tide in Knight Inlet has been found to be transferred to internal motions predominantly at the semi-diurnal frequency ( $M_2$ ) in regions of shallow topography. The internal tidal energy in Knight Inlet has been studied by many oceanographers (e.g., Webb and Pond, 1986a; Stacey, 1985; Stacey and Pond, 1992; Marsden and Greenwood, 1994). The fortnightly ( $MSf$ ) constituent which is the resultant frequency due to the beating of the  $M_2$  and  $S_2$  (whose period is very near the  $M_2$  period) constituents, has a significant influence on the inlet's low frequency, deep water circulation as shown by Baker (1992) and Baker and Pond (1995).

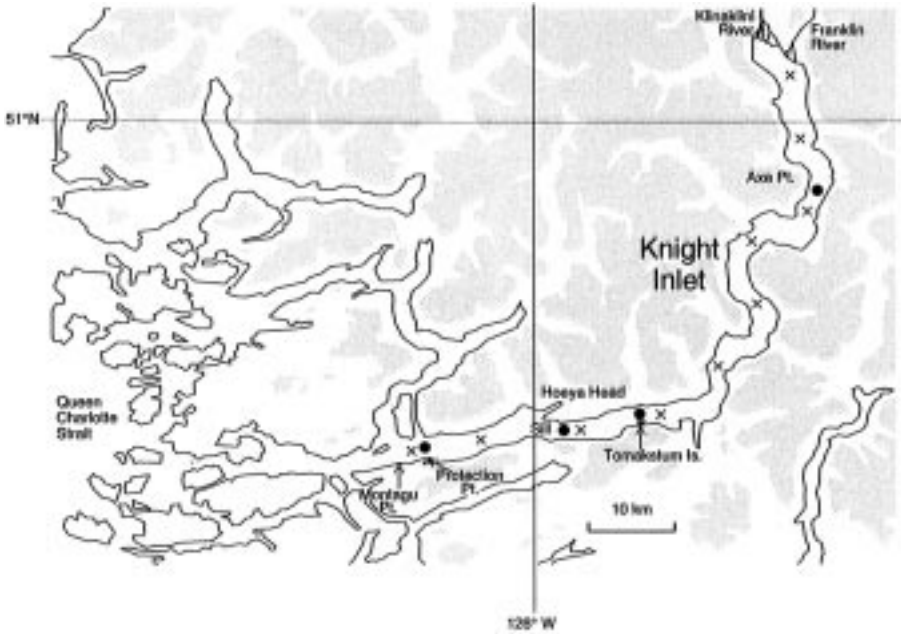


Fig. 2 Map of Knight Inlet, British Columbia. The shaded region represents elevations greater than 660 m. The “x” symbol on the map represents locations where CTD surveys have been done. The filled circles represent where moored arrays were located.

A concern of oceanographers has been whether the internal tide is reflected at the bend in Knight Inlet. Using current meter data, Farmer and Freeland (1983) estimated a reflection co-efficient of 0.9 which was later modified to 0.7 (Freeland, 1984). In contrast, Blackford (1984) estimated from CTD data that the reflection coefficient is no larger than 0.4. Webb and Pond’s (1986b) theoretical study showed that the bend in Knight Inlet should not substantially affect the propagation of the internal tide and that the reflection coefficient should be less than one percent. Marsden and Greenwood (1994) used Acoustic Doppler Current Profiler (ADCP) velocity data to estimate a reflection coefficient of 0.66, which is close to the value of Freeland (1984). It is also close to a value that can be calculated from the simulation of Stacey and Pond (1992), who developed a two-dimensional model that did not even take the bend in the inlet into account. The model, however, does take changes in the cross-sectional area along the inlet into account. As the internal tide propagates away from the sill it encounters a significant increase in cross-sectional area near the bend, and it appears that it is this increase in cross-sectional area, and not the bend itself, that is responsible for the reflection.

Many non-linear oceanographic phenomena have been observed in Knight Inlet including tidal bores, lee waves, solitons and hydraulic jumps (e.g., Farmer and Smith, 1980; Gargett, 1980; Farmer and Freeland, 1983). Much of the energy for

## Simulation of Temperature, Salinity and Velocity Fields / 5

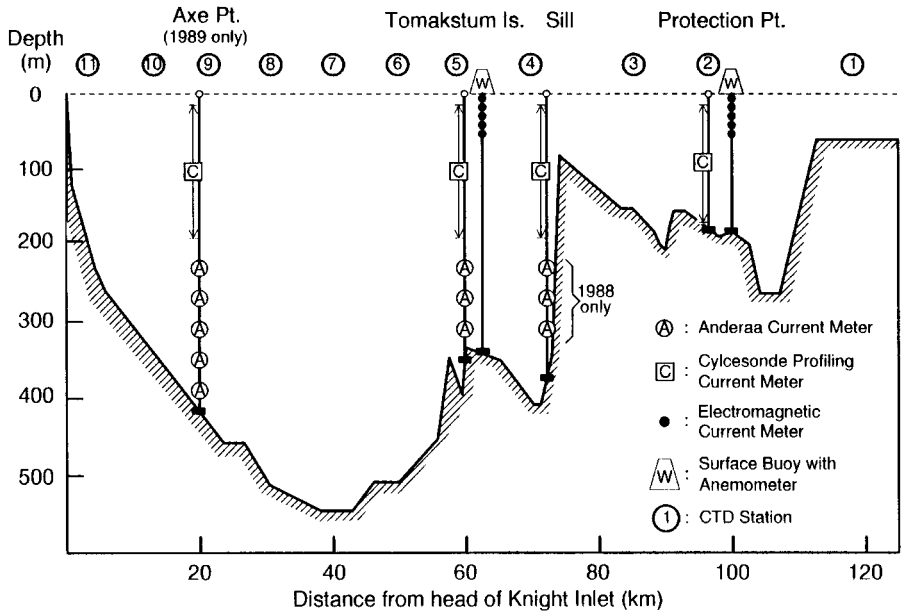


Fig. 3 Schematic plot representing the sensor positions in relation to the bathymetric features of Knight Inlet, British Columbia. Distances are measured from the head of the inlet (adapted from Baker, 1992).

producing these phenomena comes from the barotropic tide as the flow oscillates back and forth across the sill.

Baker (1992) found that there were two circulation systems situated at different depths in the inner basin. He found a shallow circulation system characterized by the outflow of brackish water on the surface with a return flow into the inlet directly below it. The other main circulation system was typified by inflow into the inlet at a depth of approximately 150 m with compensating outflows above and below the inflow region. Baker's work also indicated that bottom water displacement in the inner (outer) basin was enhanced during spring (neap) tides. His work indicated that once the deep water in the inner basin was displaced, the outer basin's deep water was more likely to be displaced, particularly during a neap tide.

Two-dimensional numerical models (Lavelle et al., 1991; Gillibrand et al., 1995; Stacey et al., 1995 are recent examples) have successfully modelled many aspects of the circulation observed in narrow inlets. Puget Sound is a complex estuary which is comprised of several interconnected branches, and Lavelle et al. (1991) developed a two-dimensional, laterally integrated model which incorporated effects due to these channels. The water density was approximated as a linear function of salinity and the vertical diffusion coefficients were empirically determined by comparing the modelled and measured salinity distributions. The advective terms in

the momentum balance were set to zero. They concentrated their study on the subtidal circulation in Puget Sound, although the tides were simulated as an integral part of the total circulation. Forces due to the wind, tide and freshwater runoff were taken into account.

Gillibrand et al. (1995) modelled Loch Sunart in Scotland. This estuary has nominally six sills with depths as small as 25 m and receives very little runoff. The model differed from that of Lavelle et al. (1991) primarily in that it did not take into account branching channels but did use the Mellor and Yamada (1982) turbulence closure scheme to prescribe the eddy diffusion parameters. Also, the free surface was allowed to move through the computational grid so that the vertical grid spacing near the surface could be less than the maximum tidal range. This model yielded reasonable estimates of the timing of deep water intrusions although their strength was significantly overestimated. This overestimation was attributed to the coarse grid resolution used in the model.

Stacey et al. (1995) modelled Knight Inlet in British Columbia, by solving for the velocity and density fields as a function of time. Temperature and salinity observations were used to construct the initial sigma-t field (and the time series of sigma-t at the open boundary) from the equation of state (Gill, 1982). The sigma-t field was allowed to evolve with the velocity field and surface displacement as a function of time. Since there is a distinct surface layer in Knight Inlet during the freshet, their model used a computational grid which was able to resolve this surface layer. Tidal displacements in the sea surface height were accounted for by utilizing a "quasi-Cartesian" coordinate system which allowed the grid to move vertically with the sea-surface. The level 2.5 Mellor-Yamada turbulence closure scheme was used. They compared their model to a particularly comprehensive set of observations (a portion of which is used in this paper) and found that the internal tide could be quite realistically simulated. The near-surface velocity field was noticeably better simulated when wind forcing was taken into account.

In this paper the model of Stacey et al. (1995) is enhanced by solving for the temperature and salinity fields separately. Even in coastal inlets where temperature may have only a minor influence on the density field, it can be important to understand and to be able to simulate the temperature field because of its influence on the biology and/or chemistry of the inlet. The enhanced model described in this paper, now called the STV model (simulates Salinity, Temperature and Velocity) will be compared to that of Stacey et al. (1995), now called the DV model (simulates Density with pressure effects removed and Velocity) and to the observations. In particular, the ability of the model to simulate the internal tide and the mean circulation will be examined. Additionally, this paper will demonstrate regions where the STV model may be more suitable than the DV model.

Both the DV and the STV models use the level 2.5 turbulence closure scheme of Mellor and Yamada (1982) where the eddy diffusion coefficients are taken to be proportional to the product of a length scale and a velocity scale. The length scale is prescribed, but a differential equation which requires boundary conditions

## Simulation of Temperature, Salinity and Velocity Fields / 7

TABLE 1. Sampling intervals and locations of the 1989 Knight Inlet data. The \* denotes a burst mode. In the burst mode, eighteen contiguous one-minute averages are recorded every hour.

Instrument	Averaged Time per sample (min)	Sample Interval (min)	Stations	Depths (m)
Anemometer	–	15	PRT, TOM	–4
S4	1	5	PRT, TOM	2, 6, 12
S4*	18 × 1	60	PRT, TOM	4, 9
Cyclesonde	–	180	PRT, SIL, TOM, AXE	15 – 190
Aanderaa	–	10	SIL, TOM, AXE	230, 270, 310
Aanderaa	–	10	AXE	350, 390

is solved for the turbulent velocity scale. At the surface, Mellor and Yamada (1982) set the turbulent kinetic energy (which is proportional to the square of the turbulent velocity scale) proportional to the friction velocity squared. This boundary condition is the one most often used by modellers. Craig and Banner (1994), however, use a surface boundary condition in which the vertical diffusive flux of turbulent kinetic energy is set proportional to the cube of the friction velocity. In this paper, visual and error estimate comparisons are made between the simulations of the internal tide produced by the Mellor and Yamada (1982) and the Craig and Banner (1994) boundary conditions. Stacey and Pond (1997) compared these two boundary conditions with their DV model and found that the mean density and horizontal velocity were more similar to the observed data if the Craig and Banner boundary condition was used. They found that the sub-tidal, residual variance (with the mean removed) between the model and the observations was generally smaller (larger) for velocity (density) when the Craig and Banner boundary condition was used.

## 2 Data

Vertical moored arrays were located at four locations in 1989 (see Fig. 3) for approximately thirty days. These stations were located at Protection Point (PRT), Tomakstum Island (TOM), the inner sill location (SIL) near Hoeya Head (see Fig. 2) and at Axe Point (AXE). These arrays measured salinity, temperature and horizontal current velocity at underwater depths which are specified in Table 1. (A similar dataset was collected in March 1988, but the temperature sensor failed in the cyclesonde at Tomakstum Island, so it will not be discussed further.) Table 1 lists the devices, sensor positions and sampling rates in the 1989 experiment. A cyclesonde profiling current meter sampled depths from 15–190 m. Aanderaa RCM-4 and RCM-7 current meters were used at depths greater than 230 m and were spaced 40 m apart to a depth of 390 m. The surface layer was sampled every 2 m by Inter-Ocean S4 electromagnetic current meters hung from buoys at TOM and PRT. One minute averages were recorded on the S4 meters from data which had a sampling frequency of 2 Hz. Alternate S4 meters recorded in a burst mode, in order to determine if there was an aliasing problem (Baker, 1992). At the moored

## 8 / Maureen L. Jeremy and Michael W. Stacey

TABLE 2. Tidal constituents used in the harmonic analysis of the data.

Constituent	Period (hours)
$MS_4$	6.10
$M_4$	6.21
$MK_3$	8.18
$S_2$	12.00
$M_2$	12.42
$N_2$	12.66
$K_1$	23.93
$P_1$	24.07
$O_1$	25.82
$MSf$	354.4
$Z_0$	$\infty$

stations, TOM and PRT, the air temperature and wind velocity were measured from either a J-Tech or Aanderaa Meteorological station which was attached to the buoy.

CTD surveys were conducted at several locations in the inlet (see Fig. 3) at the start and end of the experiment. Daily freshwater flux rates were obtained from Environment Canada for the Klinaklani River. Tidal height data at the open boundary was reconstructed from tidal constituent information (e.g., Freeland and Farmer, 1980) from Montagu Point (see Fig. 2) which is located near the mouth of the inlet.

The anemometer failed to function in 1989 at PRT. The PRT wind dataset was reconstructed by Baker (1992) based on the anemometer data from TOM and an analysis which indicated that wind magnitudes from the two stations during a similar experiment in 1988, were highly correlated with each other. The PRT and SIL cyclesondes were not functional for about the latter half of the experiment. The missing 1989 PRT temperature and salinity data which are needed to provide input at the open boundary of the numerical model were estimated by doing a harmonic analysis (Foreman et al., 1979; Foreman, 1977) of the existing data, and using the harmonic constants to extend the time series. The same technique was used by Stacey et al. (1995) for the boundary condition data at the open boundary. The open boundary condition data used in the model was the real data prior to the equipment failure followed by the extrapolated data.

The constituents used in the harmonic analysis are listed in Table 2. Modelled and measured results will be shown for only the main constituents; the semi-diurnal ( $M_2$ ), the diurnal ( $K_1$ ), the fortnightly ( $MSf$ ), the major shallow water constituent ( $M_4$ ) and the mean ( $Z_0$ ). The surface elevation data used to force the model at the open boundary was reconstructed from the  $S_2$ ,  $M_2$ ,  $N_2$ ,  $K_1$ ,  $P_1$  and  $O_1$  constituents using data from the Montagu Point tidal gauge data (Freeland and Farmer, 1980). The reconstructed PRT 1989 temperature and salinity data were calculated using the  $Z_0$ ,  $MSf$ ,  $O_1$ ,  $K_1$ ,  $S_2$ ,  $M_2$ ,  $M_4$  and  $MS_4$  constituents.

### 3 Circulation Model

#### a The Equations

The model presented in this paper is an extension of the model of Stacey et al. (1995). The laterally integrated equations in Cartesian coordinates are

$$\begin{aligned} \frac{\partial(Bu)}{\partial t} + \frac{\partial}{\partial x}(Bu^2) + \frac{\partial}{\partial z}(Buw) = \\ -\frac{B}{\rho} \frac{\partial p}{\partial x} + \frac{\partial}{\partial x} \left( BA_H \frac{\partial u}{\partial x} \right) + \frac{\partial}{\partial z} \left( BA_V \frac{\partial u}{\partial z} \right) - c_f u |u| \end{aligned} \quad (1)$$

$$\frac{\partial p}{\partial x} = \rho g \frac{\partial \eta}{\partial x} + g \int_{-\eta}^z \frac{\partial \rho}{\partial x} dz' \quad (2)$$

$$\frac{\partial(BS)}{\partial t} + \frac{\partial}{\partial x}(BuS) + \frac{\partial}{\partial z}(BwS) = \frac{\partial}{\partial x} \left( BK_H \frac{\partial S}{\partial x} \right) + \frac{\partial}{\partial z} \left( BK_V \frac{\partial S}{\partial z} \right) \quad (3)$$

$$\frac{\partial(BT)}{\partial t} + \frac{\partial}{\partial x}(BuT) + \frac{\partial}{\partial z}(BwT) = \frac{\partial}{\partial x} \left( BK_H \frac{\partial T}{\partial x} \right) + \frac{\partial}{\partial z} \left( BK_V \frac{\partial T}{\partial z} \right) \quad (4)$$

$$\frac{\partial(Be)}{\partial t} + \frac{\partial}{\partial x}(Bue) + \frac{\partial}{\partial z}(Bwe) = BS_e + \frac{\partial}{\partial x} \left( B\lambda_H \frac{\partial e}{\partial x} \right) + \frac{\partial}{\partial z} \left( B\lambda_V \frac{\partial e}{\partial z} \right) \quad (5)$$

$$w(x, z, t) = \frac{1}{B} \frac{\partial}{\partial x} \int_{z'}^H Bu dz' \quad (6)$$

$$\frac{\partial \eta}{\partial t} = W_f - \frac{1}{B} \frac{\partial}{\partial x} \left( \int_{-\eta}^H Bu dz' \right) \quad (7)$$

$$\rho = \rho(S, T, 0) \quad (8)$$

where  $T(x, z, t)$ ,  $S(x, z, t)$ ,  $u(x, z, t)$ ,  $w(x, z, t)$ ,  $\eta(x, t)$ ,  $B(x, z)$  and  $H(x)$  are the respective temperature, salinity, horizontal current velocity, vertical current velocity,

surface displacement, cross-channel width and bottom depth relative to mean sea level;  $W_f(x, t)$  is the freshwater runoff vertical velocity;  $A_H$ ,  $A_V$ ,  $K_H$ ,  $K_V$ ,  $\lambda_H$  and  $\lambda_V$  are the horizontal and vertical eddy diffusion coefficients, and  $p(x, z, t)$  and  $\rho(x, z, t)$  are the pressure and density respectively. Here,  $W_f$  is determined from freshwater flux rate data (provided by Environment Canada) and the surface area of the inlet. The sidewall drag coefficient,  $c_f$  used in this paper is identical to the one used in the model of Stacey et al. (1995).

Potential temperatures are not used here in place of  $T$  since the difference between the two is small for a relatively shallow water environment like Knight Inlet. The equation of state (8) with pressure effects removed is calculated from the empirical formula found in Gill (1982).

The level 2.5 turbulence closure model of Mellor and Yamada (1982) involves the determination of two parameters;  $e = q^2/2$  where  $q$  is the turbulent velocity scale, and  $l$ , the turbulent length scale. The length scale is prescribed below (see Eq. 10) and  $e$  requires the differential equation (5). The term  $S_e$  in (5) is the turbulent kinetic energy source term,

$$S_e = P_s + P_b - \varepsilon \quad (9)$$

where  $P_s$ ,  $P_b$  and  $\varepsilon$  are the shear production, buoyancy production and dissipation rates of turbulent energy respectively.

The model uses the same length scale,  $l$ , as Stacey et al. (1995), which is similar to that of Smith and Takhar (1981). It is prescribed as

$$l = 0.105(H + \eta) \operatorname{erf} \left[ \frac{\kappa}{0.105} \frac{\sqrt{\pi}}{2} \frac{(H - z)}{(H + \eta)} \right] \operatorname{erf} \left[ \frac{\kappa}{0.105} \frac{\sqrt{\pi}}{2} \frac{(z + \eta)}{(H + \eta)} \right] \quad (10)$$

where  $\kappa$  is von Kármán's constant ( $\kappa = 0.4$  in the model). Near the upper and lower boundaries,  $l$  increases linearly toward the interior, while, away from these boundaries,  $l \approx 0.105(H + \eta)$ . Note that a roughness length has not been included in (10). It is assumed to be zero in this paper.

In the turbulence model of Mellor and Yamada (1982), the vertical diffusion coefficients are prescribed as follows;

$$A_V = lqS_M \quad K_V = lqS_H \quad \lambda_V = lqS_q \quad (11)$$

where  $S_M$ ,  $S_H$  and  $S_q$  are stability functions. The vertical diffusion terms,  $A_V$  and  $K_V$  are restricted to the minimum value of

$$A_{V_{min}} = K_{V_{min}} = a_0 N^{-1.5} \quad (12)$$

where  $a_0$  depends on the characteristic internal wave field (here  $a_0 = 3.1 \times 10^{-4} \text{ cm}^2 \text{ s}^{5/2}$ ) and  $N$  is the Brunt-Väisälä frequency (Stacey et al., 1995).

The horizontal eddy viscosity terms used by Stacey and Pond (1992) and Stacey et al. (1995) were also used in this model where

## Simulation of Temperature, Salinity and Velocity Fields / 11

$$A_H = \frac{(\Delta x)^2}{T_A}, \quad K_H = \frac{(\Delta x)^2}{T_K}, \quad \lambda_H = \frac{(\Delta x)^2}{T_\lambda}, \quad (13)$$

$\Delta x$  is the horizontal grid spacing and  $T_A$ ,  $T_K$  and  $T_\lambda$  are time constants which have respective values of 100 h, 1000 h, and 100 h. These values are not empirically derived, and were chosen so that the diffusion rates would be very slow relative to the tidal cycle. Sensitivity studies of these time constants can be found in Stacey et al. (1995).

Stacey et al. (1995) found, following Smagorinsky (1963), that in order to prevent nonlinear instabilities in regions of steep topography, an extra diffusion term of the form

$$\frac{\partial}{\partial x} \left[ \gamma \Delta x^2 \left| \frac{\partial(Bu)}{\partial x} \right| \left| \frac{\partial(\zeta)}{\partial x} \right| \right] \quad (14)$$

had to be included in the differential equations for  $\zeta = u$ ,  $\rho$  and  $e$ . For the model presented here (14) is included in the differential equations for  $\zeta = u$ ,  $S$ ,  $T$  and  $e$ . Here and in the model of Stacey et al. (1995) the constant  $\gamma$  was set equal to 0.2.

The equations were transformed into the quasi-Cartesian  $(x, \hat{z}, t)$  coordinate system where

$$\frac{\hat{z}}{H} = \frac{z + \eta}{H + \eta} \quad \begin{array}{l} 0 \leq \hat{z} \leq H \\ -\eta \leq z \leq H \end{array} \quad (15)$$

This  $\hat{z}$  coordinate transformation permits very fine resolution near the surface even though the surface height varies by several metres due to the tide. The numerical errors that can occur with sigma coordinates in regions of steep bottom topography as shown by Haney (1991) do not occur with the  $\hat{z}$  transformation. This is because the sigma coordinate positions vary predominantly with the bottom profile while the  $\hat{z}$  coordinate positions nearly parallel the surface. Consequently, lines of constant  $\hat{z}$  are almost the same as constant  $z$ .

A mode-splitting technique was used whereby the barotropic and baroclinic velocities were calculated separately and at different time steps. The technique was the same as the one used by Stacey et al. (1995) except that  $S$  and  $T$  were calculated separately (instead of density), and then density was calculated using the equation of state.

The staggered computational grid has ninety positions for each dependent variable in the horizontal and a maximum of forty-five positions in the vertical direction (Fig. 4). The positions of the grid points were chosen so that: a) the thin surface, freshwater layer could be resolved; and b) the steep topography in the region of the sill could be resolved. Salinity and temperature were calculated at the grid locations shown in Fig. 4.

The spatial numerical finite difference method used was the centred difference scheme while the scheme used for the time integrations, was the Huen scheme (Mesinger and Arakawa, 1976). Both schemes have second order accuracy.

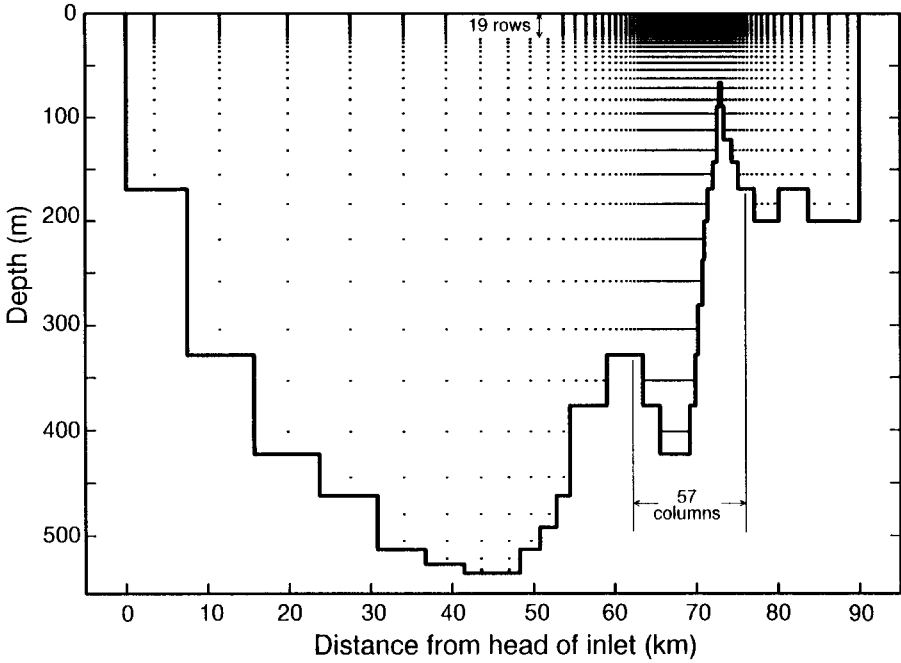


Fig. 4 The grid positions of the salinity and temperature parameters.

**b** *Boundary Conditions*

Normal to the inlet's bottom and lateral boundaries, the heat flux and velocity are set to zero. However parallel to the surface and based on the quadratic drag law, the bottom stress,  $\tau_b$ , is

$$\tau_b = \rho c_d |u_b| u_b = -\rho A_V \frac{\partial u}{\partial z} \Big|_{z=H} \tag{16}$$

where  $u_b$  is the horizontal velocity near the bottom. The surface stress,  $\tau_w$ , at the air-sea interface is

$$\tau_w = \rho_a c_w |W| (W - u) = -\rho A_V \frac{\partial u}{\partial z} \Big|_{z=-\eta} \tag{17}$$

where  $W$  is the wind velocity parallel to the surface and  $\rho_a$  is the air density. Stacey et al. (1995) included the water velocity,  $u$  in (17) so that the surface stress at the interface would equal zero when the wind velocity equalled the surface water velocity. Here  $c_d$  and  $c_w$  are the respective drag coefficients for the ocean-bottom and ocean-air interfaces. For the simulations in Stacey et al. (1995) and in this paper,  $c_d$  has been set to 0.003 while  $c_w$  has been set to 0.0011.

## Simulation of Temperature, Salinity and Velocity Fields / 13

Two surface turbulent kinetic energy boundary conditions are compared in this study. These are referred to as the Mellor-Yamada boundary condition (BCMY) proposed by Mellor and Yamada (1982), and the Craig-Banner boundary conditions (BCCB) proposed by Craig and Banner (1994). The BCMY was used for the Stacey et al. (1995) model.

For the BCMY, the assumption is made that near boundaries the turbulent kinetic energy production equals the dissipation rate. The boundary condition (Mellor and Yamada, 1982) can then be shown to be

$$q^2 = B_1^{2/3} u_*^2 \quad (18)$$

where  $u_* = (\tau/\rho)^{1/2}$  is the friction velocity,  $\tau$  is the stress near the boundary, and  $B_1 = 16.6$ .

For the BCCB, the influence of surface waves is taken into account, leading Craig and Banner (1994) to propose the flux condition,

$$\lambda_v \left. \frac{\partial e}{\partial z} \right|_{z=-\eta} = \alpha u_*^3. \quad (19)$$

where  $\alpha = 100$ . Craig and Banner (1994), and Craig (1996) used either this value for  $\alpha$ , or values of the same order, based on results from spectral wave models. Further parametrization studies which include the value of  $\alpha$ , can be found in Craig (1996).

At the open boundary (e.g., at the inlet mouth) when there is outflow, the radiation equations

$$\frac{\partial \zeta}{\partial t} + u \frac{\partial \zeta}{\partial x} = 0 \quad (20)$$

are used where  $\zeta$  indicates one of  $u$ ,  $S$ ,  $T$  or  $q^2$ . The boundary conditions at the open boundary during inflow conditions are: 1) the horizontal velocity gradients become zero; 2) the  $S$ ,  $T$  boundary conditions are equal to the data from PRT; and 3)  $q^2$  is set to a small number of  $O[10^{-1}] \text{ cm}^2 \text{ s}^{-2}$ . At solid boundaries,  $q$  and the fluxes of  $T$  and  $S$  are set to zero.

Due to the flux of fresh water,  $W_f$  (Eq. 7) the surface boundary condition

$$W_f(S_s - S_f) = -K_v \left. \frac{\partial S}{\partial z} \right|_{-\eta} \quad (21)$$

is imposed on the salt flux where  $S_s$  and  $S_f$  are the respective surface and freshwater inflow salinity. Here,  $S_f$  was always taken to be zero.

Ideally, one would also like to specify the heat flux at the surface, but in practice it can be very difficult to calculate. Consequently, instead of specifying the surface heat flux, the surface temperature is imposed. This approach is the same as the method implemented in many ocean models (e.g., Semtner and Chervin, 1988).

A comparison will be made here between simulations which use this boundary condition and simulations which assume that the diffusive heat flux across the air-water interface is zero.

These imposed surface temperatures were constructed from the near surface, initial and final CTD surveys which were separated in time by about 30 days. Linear interpolations were performed both spatially and temporally to provide each grid point with input at each time step. Ideally a database which was sampled more frequently with time would have been preferable. Inspection of the S4 water temperature data indicates that the daily variation can be as large as  $10^{\circ}\text{C}$  with peak temperatures as high as  $18^{\circ}\text{C}$  occurring near midday. This daily surface temperature cycle, particularly in the summer season, has a cycle which is very near the  $K_1$  constituent. In spite of this obvious limitation, however, we will show that reasonable simulations of the temperature field can be obtained.

### 4 Results

TOM is the only station shown in this paper because it is the only station (with the exception of PRT, where the boundary data was provided) which had S4s available at shallow depths (i.e., 2 to 14 m). Since the constituent profiles (simulated data) had large variations at shallow depths, the results from stations other than TOM, were not as enlightening, nor, did they alter the conclusions reached in this paper. Comparison of the model to the observations from the other stations can be found in Yeremy (1995). In the following figures, the modelled data shown are horizontally averaged over the three nearest grid lines on the computational grid unless otherwise indicated.

The initial salinity and temperature fields for the model are shown in Figs 5 and 6. Note the existence of the distinct surface layer. Also, the salinity was lower near the head of the inlet than further downstream which indicates that mixing had occurred with distance from the freshwater source at the inlet's head. Solar heating effects are also observable from the surface temperatures. The surface water downstream ( $\approx 14^{\circ}\text{C}$  at TOM) was warmer than the upstream water ( $\approx 10^{\circ}\text{C}$  at AXE) and the temperatures in the surface layer were warmer than the more saline water directly below.

#### a Velocity

The constituent profiles for velocity are shown in Fig. 7 and in Fig. 8 the shallow depths are emphasized. In Table 3a,b, the Sum of the Square of the Residuals (SSR) between the observation and modelled data for these same constituents are provided. Also, shown in Table 4 are the normalized total residuals which are these SSR values, normalized at each depth by the observed variance of the appropriate constituent and summed over the depths between 2 and 14 m. At shallow depths, the  $K_1$  phase and  $M_4$  amplitude are significantly different from the measured data (Fig. 8d,g). Otherwise, one can see that the model has simulated the tidal response and the mean quite well. The main difference caused by the choice of boundary

## Simulation of Temperature, Salinity and Velocity Fields / 15

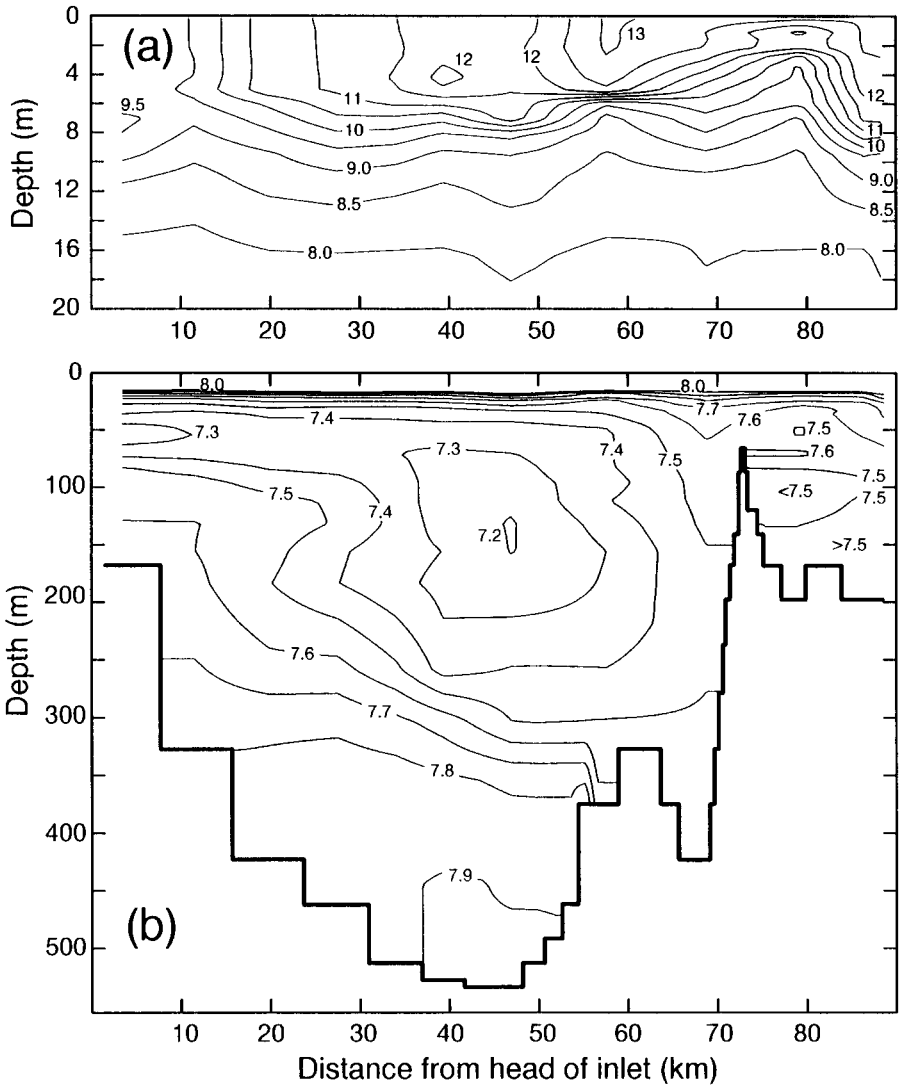


Fig. 5 The 1989 temperature profile used as the initial temperature field to the model. Panel (a) emphasizes the shallow water contours while Panel (b) shows the entire temperature field.

condition for  $q^2$  is in the magnitude and shear of the amplitude near the surface. The near surface shear is significantly less for all of the constituents when the Craig-Banner boundary condition is used. These shears appear more reasonable when compared to the larger shears, which are simulated with BCMY instead. Unfortunately, no observational data is available for depths less than 2 m where significant differences between the BCCB and BCMY simulations occur. When the

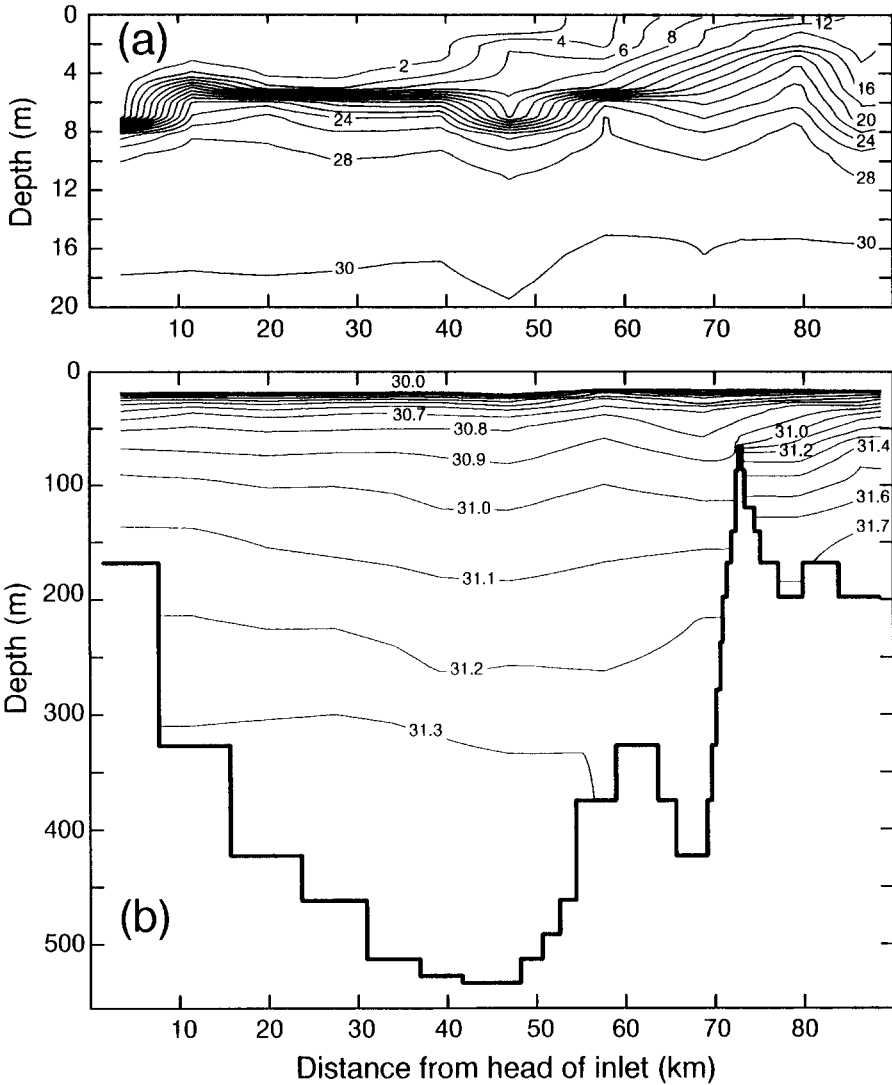


Fig. 6 The 1989 salinity profile used as the initial salinity field to the model. Panel (a) emphasizes the shallow water contours while Panel (b) shows the entire salinity field.

sum of the square of the residuals between the BCMY and BCCB simulations are compared (in Table 3a,b) the BCCB  $M_4$ ,  $MSf$  at depths 4, 12 and 14 m, and  $M_2$  at a depth of 14 m, have values less than the BCMY. However, at depths of 6 and 9 m, the BCCB  $MSf$  (SSR) values are substantially larger than the corresponding values for the BCMY modelled data. This coincides with the depths where the

## Simulation of Temperature, Salinity and Velocity Fields / 17

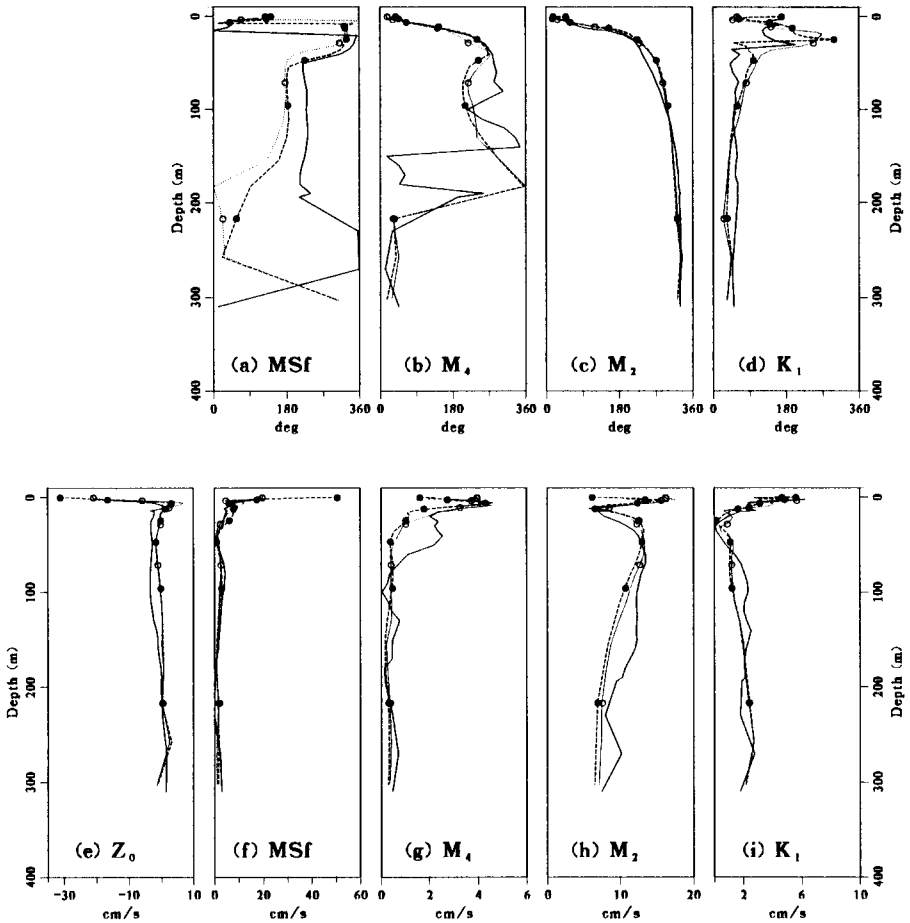


Fig. 7 TOM's velocity tidal constituent profiles: The constituent profiles calculated from the observations are the solid lines. The dashed lines with the filled circles and the dotted lines with the open circles represent the respective BCMY and BCCB modelled STV data. Figures a–d are the phases while Figs e–i are the amplitudes.

BCCB mean in Fig. 8e departs slightly more than the BCMY mean relative to the measured mean.

It is interesting to note when comparing (a) and (c) in Table 3, that the latter's sum of the square of the residuals (except *MSf*), are less in magnitude. The only difference between these two simulations is that (c) has the surface heat flux set to zero. It should be noted however, that the normalized residuals averaged over depth in Table 4 do not indicate as substantial a difference between the two different simulations. As will be demonstrated further in the text, an imposed surface temperature boundary condition results in more realistic temperature simulations

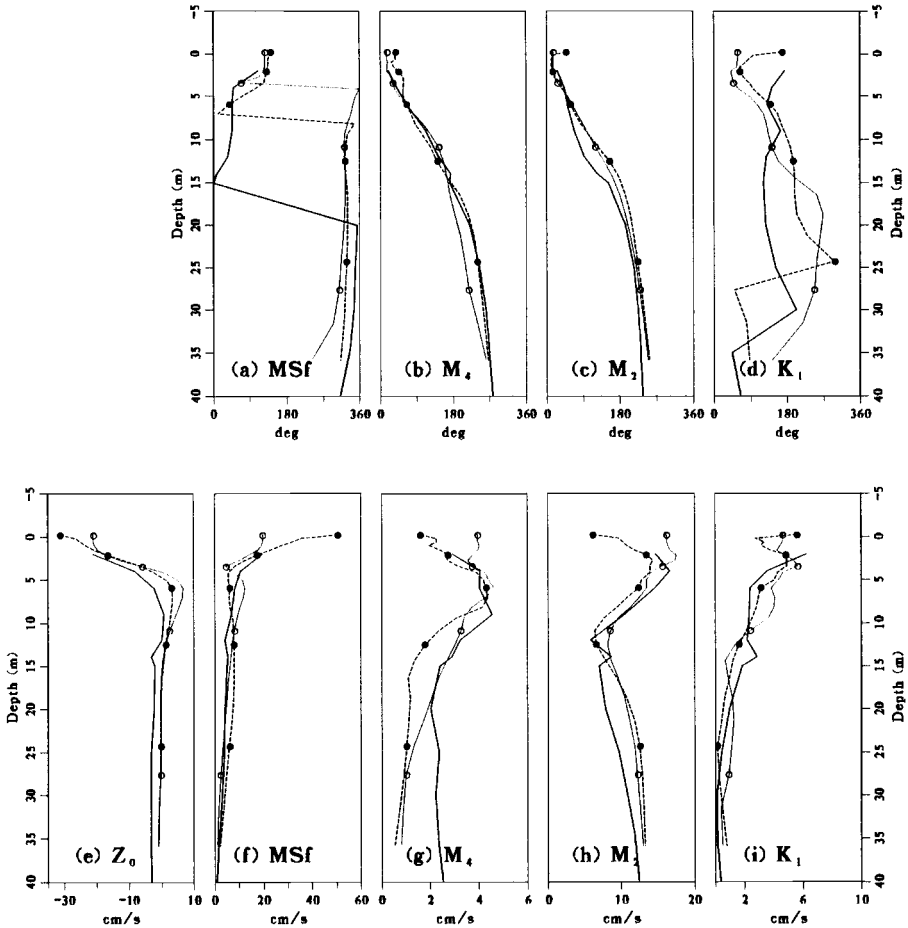


Fig. 8 The shallow depths of Fig. 7 are emphasized here.

for the mean and possibly *MSf* constituent, but not the diurnal ( $K_1$ ) and semi-diurnal ( $M_2$ ) constituents. This is consistent with these velocity results since the higher frequency velocities are not as well simulated when the surface temperature boundary condition is imposed. Also, this indicates that the velocities are slightly sensitive to temperature variations at shallow depths.

As aforementioned, one of the objectives of this paper is to determine if it is necessary to model temperature and salinity separately instead of modelling density alone. Figure 9 compares the TOM velocity results between the STV (BCMY, with the surface temperature boundary condition imposed) and DV models (BCMY). Only the shallow depths are shown since the significant differences between the two models occur there. In Fig. 9 there are visually few differences between the

## Simulation of Temperature, Salinity and Velocity Fields / 19

TABLE 3. The sum of the squares of the residuals between the observed and modelled velocity constituents, at shallow depths for models (a) STV-BCMY, (b) STV-BCCB, (c) STV-BCMY with the surface heat flux set to zero, (d) DV-BCMY

Model	Depth (m)	SSR $K_1$ ( $\text{cm}^2 \text{s}^{-2}$ )	SSR $M_2$ ( $\text{cm}^2 \text{s}^{-2}$ )	SSR $M_4$ ( $\text{cm}^2 \text{s}^{-2}$ )	SSR $MSf$ ( $\text{cm}^2 \text{s}^{-2}$ )
a	2	40.90	6.13	0.73	23.47
	4	5.86	4.93	0.60	39.89
	6	0.35	4.50	0.04	2.93
	9	0.10	12.37	1.22	29.86
	12	2.17	15.31	0.93	28.47
	14	3.93	24.22	1.20	14.56
b	2	48.87	8.14	0.39	19.76
	4	16.70	5.21	0.12	23.53
	6	1.81	4.53	0.19	59.97
	9	2.43	14.08	0.68	55.92
	12	0.38	14.74	0.13	27.09
	14	3.31	13.39	0.13	10.62
c	2	31.11	5.59	0.66	27.28
	4	6.05	6.23	1.00	38.83
	6	0.85	6.18	0.13	2.24
	9	0.18	8.63	1.03	12.56
	12	2.35	12.57	1.62	15.29
	14	4.20	23.40	2.24	6.80
d	2	29.08	12.32	0.23	19.88
	4	4.29	13.18	2.07	36.98
	6	0.65	7.22	0.32	1.63
	9	0.04	9.99	2.21	6.81
	12	1.72	15.63	1.26	11.90
	14	3.80	24.77	1.26	5.23

TABLE 4. The normalized residuals between the observed and modelled velocity constituents summed over shallow depths between 2 and 14 m, for models (a) STV-BCMY, (b) STV-BCCB, (c) STV-BCMY with the surface heat flux set to zero, (d) DV-BCMY

Model	$K_1$	$M_2$	$M_4$	$MSf$
a	5.07	1.91	0.83	6.71
b	7.63	1.64	0.25	8.74
c	4.94	1.68	1.24	3.80
d	4.08	2.04	1.10	2.94

DV and STV constituent profiles, except that the STV  $M_4$  amplitude between 2 and 14 m (Fig. 9g) is more similar to the observed data than the DV model. This is substantiated by the comparison of (d) from Table 3 with both (a) and (c). Furthermore, recall that the simulated  $M_4$  amplitude was even better modelled when the Craig-Banner boundary condition (BCCB) was used (Fig. 8g, Table 4a,b and Table 3a,b). Also, note from Table 3c,d, that the STV (with zero surface heat flux)

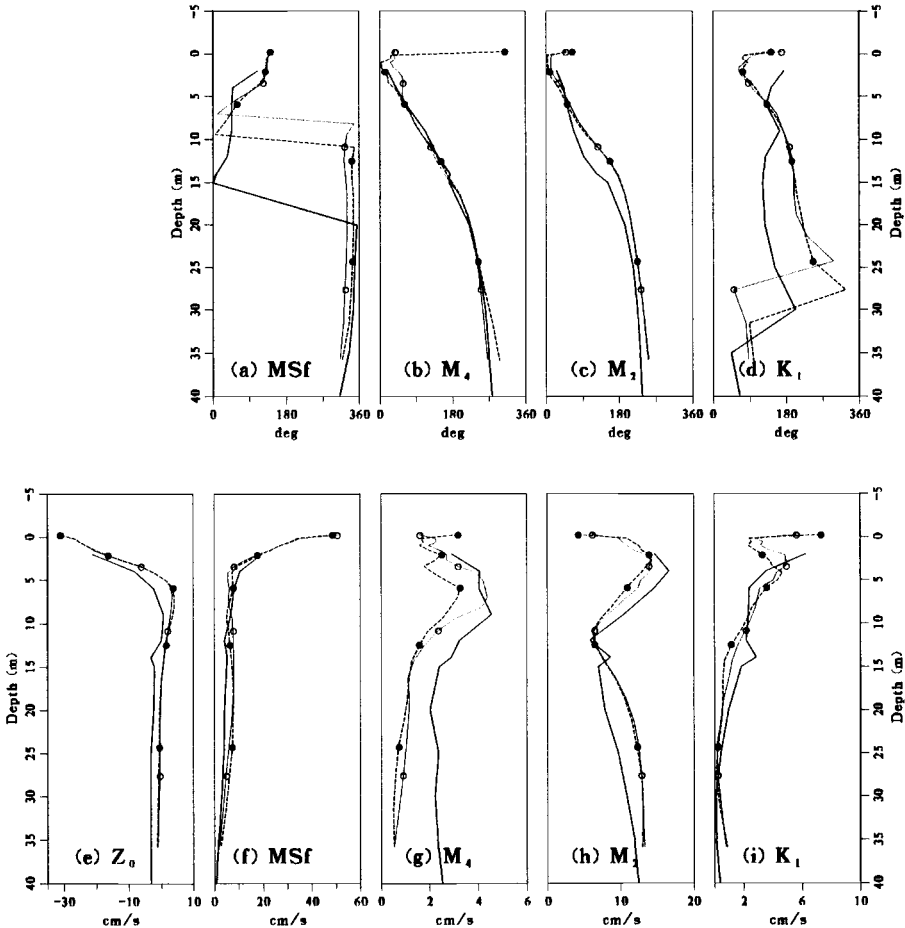


Fig. 9 TOM's velocity tidal constituent profiles: The constituent profiles calculated from the observations are the solid lines. The dashed lines with the filled circles and the dotted lines with the open circles are the modelled data from the respective DV and STV models (both BCMY). Figures a–d are the phases while Figs e–i are the amplitudes.

simulated velocities have SSRs that are smaller for the  $M_2$  constituent but larger for the  $K_1$  and  $MSf$  constituents when compared to the DV model. This indicates small differences between velocities simulated using the STV and DV models.

**b Temperature**

The constituent profiles are shown in Fig. 10 for shallow depths only, since the variation of these constituents at greater depths was small. Here, it can be seen that for the observed data, the greatest temperature perturbations occur at depths less than 25 m. Qualitatively, this characteristic is duplicated by the modelled data

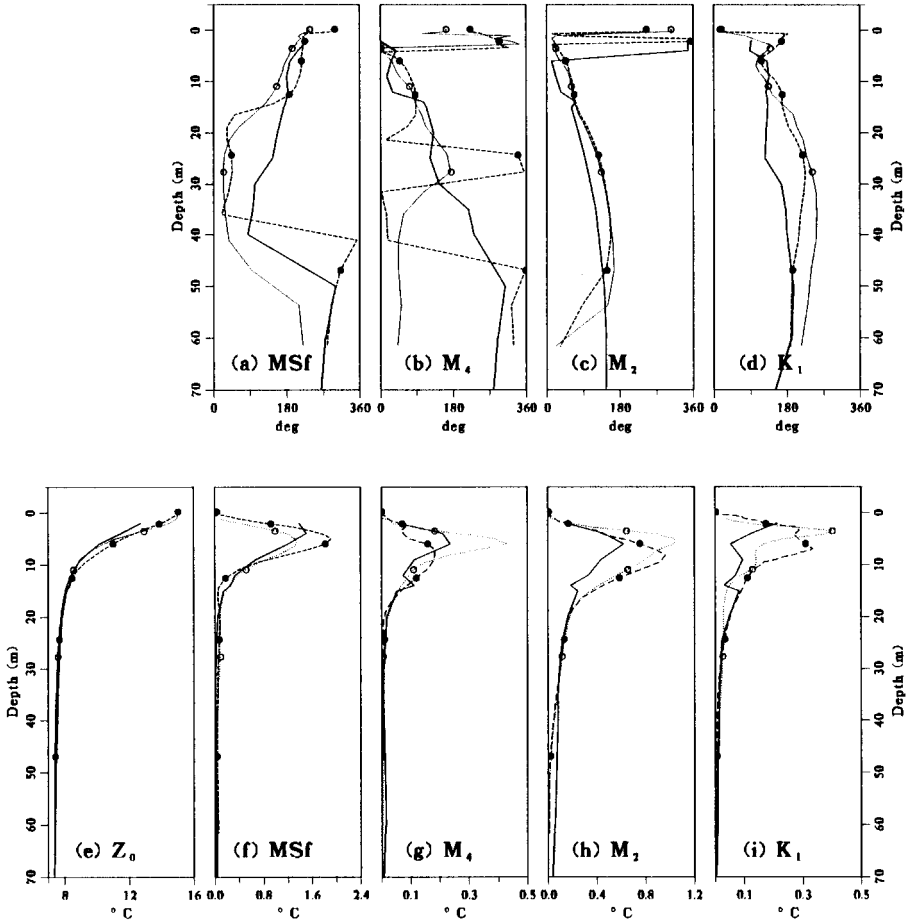


Fig. 10 TOM's temperature tidal constituent profiles: The constituent profiles calculated from the observations are the solid lines. The dashed lines with the filled circles and the dotted lines with the open circles represent the respective BCMY and BCCB modelled STV data. Figures a–d are the phases while Figs e–i are the amplitudes.

from simulations using both boundary conditions, but quantitatively the modelled amplitudes differ by a factor of about two except for the mean and perhaps the *MSf* amplitude. These modelled temperatures could probably be improved if the prescribed surface temperature was comprised of higher frequency data which included at least diurnal and semi-diurnal variations. In Fig. 10, one sees that the simulated mean and *MSf* profiles are similar to the observed mean and *MSf*, while the observed constituents at higher frequencies are not simulated as well. In Table 5, one sees that the low frequency constituent *MSf* is better modelled (smaller SSRs) when the surface temperature is imposed while the diurnal and semi-diurnal

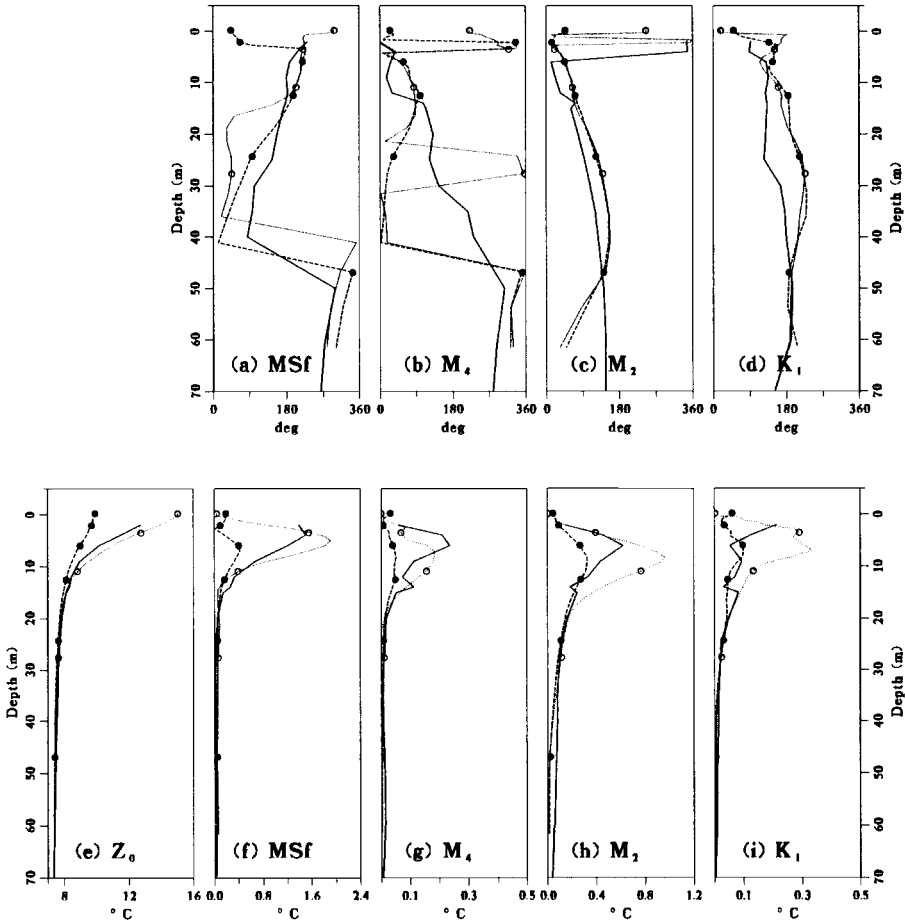


Fig. 11 TOM's temperature tidal constituent profiles: The constituent profiles calculated from the observations are the solid lines. The dashed lines with the filled circles and the dotted lines with the open circles represent the respective STV modelled data with the surface heat flux set to zero and with an imposed surface temperature boundary condition. Figures a-d are the phases while Figs e-i are the amplitudes.

constituents,  $K_1$  and  $M_2$ , are better modelled when the surface heat flux is set to zero. This result is further supported by the normalized total residuals shown in Table 6.

In Fig. 11, a comparison of the modelled temperatures (BCMY) is made between simulations which prescribe the surface temperature and those which set the surface heat flux to zero. It is immediately apparent that when the surface temperature is prescribed, one obtains much more realistic modelled temperatures for the lower frequency constituents (see also Table 5). However for the higher frequencies, such

## Simulation of Temperature, Salinity and Velocity Fields / 23

TABLE 5. The sum of the squares of the residuals between the observed and modelled temperature constituents, at shallow depths for (a) STV-BCMY, (b) STV-BCCB and (c) STV-BCMY with the surface heat flux set to zero.

Model	Depth (m)	SSR $K_1$ ( $^{\circ}\text{C}^2$ )	SSR $M_2$ ( $^{\circ}\text{C}^2$ )	SSR $M_4$ ( $^{\circ}\text{C}^2$ )	SSR $MSf$ ( $^{\circ}\text{C}^2$ )
a	2	0.028	0.000	0.002	0.152
	4	0.025	0.049	0.014	0.078
	6	0.034	0.093	0.006	0.430
	9	0.006	0.207	0.011	0.113
	12	0.003	0.081	0.006	0.006
	14	0.003	0.036	0.001	0.017
b	2	0.007	0.005	0.001	0.544
	4	0.043	0.137	0.012	0.141
	6	0.007	0.127	0.018	0.031
	9	0.001	0.122	0.005	0.031
	12	0.000	0.050	0.002	0.025
	14	0.000	0.026	0.001	0.020
c	2	0.018	0.003	0.001	1.103
	4	0.006	0.059	0.018	0.905
	6	0.001	0.090	0.021	0.398
	9	0.000	0.036	0.004	0.091
	12	0.001	0.018	0.002	0.014
	14	0.001	0.002	0.003	0.010

TABLE 6. The normalized residuals between the observed and modelled temperature constituents summed over shallow depths between 2 and 14 m, for models (a) STV-BCMY, (b) STV-BCCB and (c) STV-BCMY with the surface heat flux set to zero.

Model	$K_1$	$M_2$	$M_4$	$MSf$
a	35.79	6.77	6.08	1.97
b	12.19	6.15	3.54	1.94
c	4.33	2.15	4.34	3.46

as the diurnal constituent,  $K_1$ , Table 6 demonstrates that error is introduced when the surface temperature boundary condition is imposed (perhaps, because diurnal variations have not been included in the surface temperature boundary condition).

### c Salinity

The salinities are shown in Fig. 12 and one sees that, with the exception of the  $MSf$  constituent, the amplitude profiles are better simulated by the Craig and Banner boundary condition. This is further supported in Table 7 and Table 8. Also, as can be seen in Table 8, the  $M_2$  and  $M_4$  amplitudes are much better simulated by the

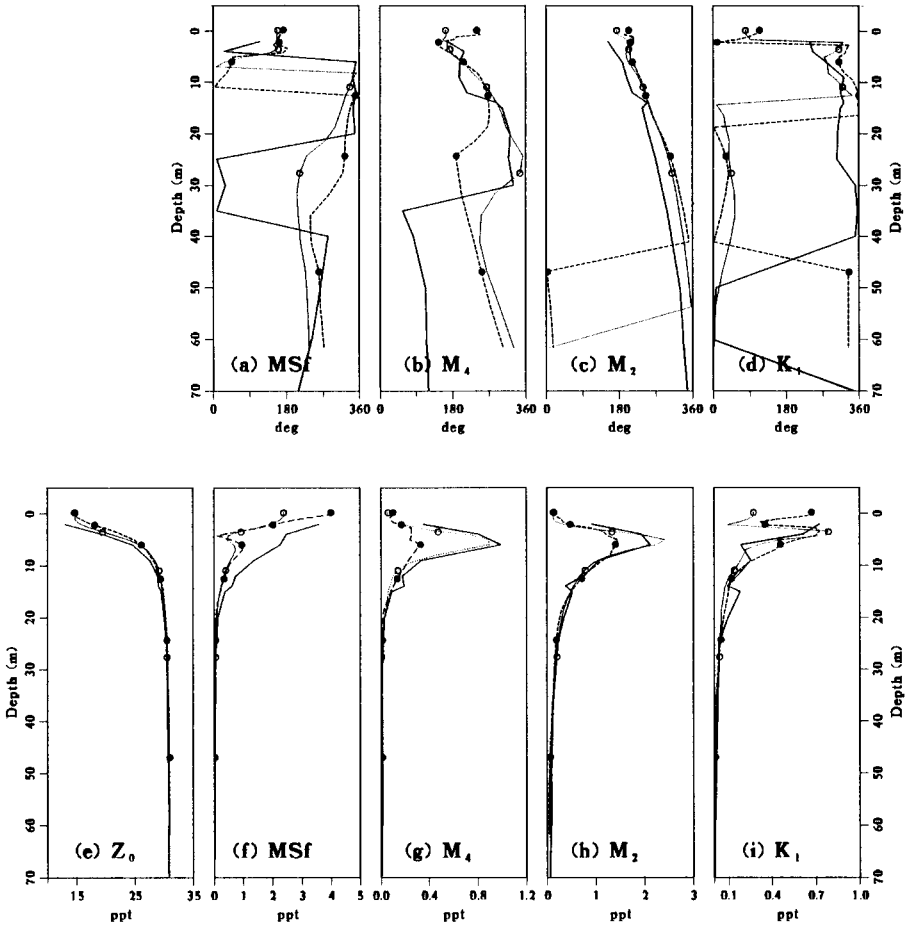


Fig. 12 TOM's salinity tidal constituent profiles: The constituent profiles calculated from the observations are the solid lines. The dashed lines with the filled circles and the dotted lines with the open circles represent the respective BCMY and BCCB modelled STV data. Figures a-d are the phases while Figs e-i are the amplitudes.

Craig and Banner boundary condition in the upper 15 m. The phases are about equally well simulated by the two boundary conditions. The  $M_4$  amplitude profile is particularly sensitive to the choice of boundary condition.

### 5 Discussion and Conclusions

In this project the numerical model of Stacey et al. (1995) has been enhanced to solve for the temperature and salinity fields in an inlet. Density is calculated from the equation of state (Gill, 1982). Therefore, the nonlinear aspects of the equation of state are represented in the difference equations. Solar heating is included by

## Simulation of Temperature, Salinity and Velocity Fields / 25

TABLE 7. The sum of the squares of the residuals between the observed and modelled salinity constituents, at shallow depths for (a) STV-BCMY and (b) STV-BCCB.

Model	Depth (m)	SSR $K_1$ ppt <sup>2</sup>	SSR $M_2$ ppt <sup>2</sup>	SSR $M_4$ ppt <sup>2</sup>	SSR $MSf$ ppt <sup>2</sup>
a	2	0.49	0.29	0.02	3.41
	4	0.36	0.76	0.20	3.67
	6	0.05	0.51	0.23	1.65
	9	0.00	0.18	0.03	0.48
	12	0.01	0.08	0.01	0.07
	14	0.00	0.02	0.01	0.07
b	2	0.28	0.27	0.02	3.07
	4	0.20	0.45	0.11	3.90
	6	0.01	0.16	0.01	1.49
	9	0.01	0.12	0.03	0.33
	12	0.00	0.07	0.01	0.09
	14	0.00	0.01	0.01	0.08

TABLE 8. The normalized residuals between the observed and modelled salinity constituents summed over shallow depths between 2 and 14 m, for models (a) STV-BCMY and (b) STV-BCCB.

Model	$K_1$	$M_2$	$M_4$	$MSf$
a	7.50	2.23	2.96	3.50
b	3.34	1.62	2.17	3.50

prescribing the temperature at the surface. This project also investigated the difference between two turbulent kinetic energy boundary conditions; Mellor-Yamada (1982) and Craig-Banner (1994).

The model simulates the tidal component of the temperature and salinity signal reasonably well at most depths. The salinities are particularly realistic (Fig. 12) when the Craig-Banner boundary condition is used. Temperatures near the surface are more realistic when solar heating is included (Fig. 11) through an imposed surface temperature. However, at diurnal and higher frequencies, the near surface modelled temperatures are not as similar to the observed temperature profiles as the constituents at lower frequencies (mean and  $MSf$ ). This may be due to the sparse data available for the surface temperature boundary condition which was estimated from CTD surveys taken thirty days apart. It is possible that the simulated surface temperatures would improve if the boundary condition was comprised of higher frequency components.

The model which simulated density and the model which simulated salinity and temperature instead were compared and the two models produced similar velocity

profiles. One exception is that the  $M_4$  amplitude is better modelled at depths between 2–12 m when salinity and temperature are treated separately. (It should be noted that the  $M_4$  amplitude improves even more if the Craig-Banner boundary condition is used.) There are indications that the shallow water velocities in the STV model were slightly sensitive to temperature since the two different boundary conditions for temperature produced somewhat different velocity profiles. However, this study indicates that models of inlets like Knight Inlet which use the density parameter instead of salinity and temperature, produce reasonable simulations of the velocity field.

In conclusion, there is reasonable agreement between the observed and simulated salinity and temperature tidal constituents using the model described in this paper. The velocity tidal constituents are also modelled reasonably well and are very similar to simulations from a previous model (Stacey et al., 1995). The previous model simulated density while the model in this paper treated salinity and temperature separately. The inclusion of solar heating by prescribing the surface temperature resulted in better modelled temperatures, particularly for the lower frequency constituents, than when the heat flux was set to zero. It is expected that better simulations of the temperature could be attained if a more complete set of boundary data were available.

The Craig-Banner surface boundary condition for the turbulent kinetic energy condition has been shown to produce noticeably different velocity, temperature and salinity profiles at tidal frequencies than the more commonly used Mellor-Yamada boundary condition. Even though the Craig-Banner boundary condition was developed with wind-forced flows in mind (and wind-forcing is included in this model), in a few cases it produces tidal simulations that more closely resemble the observations (e.g., the  $M_4$  and  $M_2$  salinity profiles). Also, the near surface shears in velocity are smaller when the Craig-Banner boundary condition is used. This suggests to us that the Craig-Banner boundary condition is a viable alternative to the Mellor-Yamada boundary condition.

---

## References

- BAKER, P.D. 1992. Low frequency residual circulation in Knight Inlet, a fjord of coastal British Columbia, M.Sc. thesis, University of British Columbia, Vancouver, B.C., Canada. 184pp.
- and POND, S. 1995. The low frequency residual circulation in Knight Inlet, British Columbia. *J. Phys. Oceanogr.*, **25**: 747–763.
- BLACKFORD, B.L. 1984. Effect of a tidal stream on internal wave observations and predictions. *ATMOSPHERE-OCEAN*, **22**: 125–143.
- CRAIG, P.D. 1996. Velocity profiles and surface roughness under breaking waves. *J. Geophys. Res.*, **101**, No. C1: 1265–1277.
- and BANNER, M.L. 1994. Modelling wave-enhanced turbulence in the ocean surface layer. *J. Phys. Oceanogr.*, **25**: 2546–2559.
- EMBLETON, C. and KING, C.A.M. 1968. *Glacial and Periglacial Geomorphology*, Edward Arnold, 585 pp.
- FARMER, D.M. and SMITH, J.D. 1980. Generation of the lee waves over the sill in Knight Inlet, In: *Fjord Oceanography*, Freeland, H.J., Farmer,

## Simulation of Temperature, Salinity and Velocity Fields / 27

- D.M. and Levings, C.D. (Eds) Plenum Press, pp. 259–269.
- and FREELAND, H.J. 1983. The physical oceanography of fjords. *Prog. Oceanogr.*, **12**(2): 147–219.
- FOREMAN, M.G.G. 1977. Manual for tidal heights analysis and prediction, *Pacific Marine Science Report 77-10*, Institute of Ocean Sciences, Patricia Bay, Sidney, B.C., 97 pp.
- and HENRY, R.F. 1979. Tidal analysis based on high and low water observations, *Pacific Marine Science Report 79-15*, Institute of Ocean Sciences, Patricia Bay, Sidney, B.C., 39 pp.
- FREELAND, H.J. 1984. The partition of internal tidal motions in Knight Inlet, British Columbia. *ATMOSPHERE-OCEAN*, **22**(2): 144–150.
- and FARMER, D.M. 1980. Circulation and energetics of a deep, strongly stratified inlet. *Canadian J. Fisheries and Aquatic Science*, **37**: 1398–1410.
- GARGETT, A. 1980. Turbulence measurements through a train of breaking internal waves in Knight Inlet, B.C., In: *Fjord Oceanography*, Freeland, H.J., Farmer, D.M. and Levings, C.D. (Eds) Plenum Press, N.Y., pp. 277–282.
- GILL, A.E. 1982. *Atmosphere-Ocean Dynamics*, Academic Press, New York, N.Y., 643 pp.
- GILLIBRAND, P.A.; TURRELL, W.R. and ELLIOT, A.J. 1995. Deep-water renewal in the upper basin of Loch Sunart, a Scottish fjord. *J. Phys. Oceanogr.* **25**(6): 1488–1503.
- HANEY R.L. 1991. On the pressure gradient force over steep topography in sigma coordinate ocean models, *J. Phys. Oceanogr.*, **21**: 610–619.
- LAVELLE, J.W.; COKELET, E.D. and CANNON, G.A. 1991. A model study of density intrusions into and circulation within a deep, silled estuary: Puget Sound. *J. Geophys. Res.* **96**(C9): 16770–16800.
- MARSDEN, R.F. and GREENWOOD, K.C. 1994. Internal tides observed by an acoustic Doppler current profiler. *J. Phys. Oceanogr.* **24**(6): 1097–1109.
- MELLOR, G.L. and YAMADA, T. 1982. Development of a turbulence closure model for geophysical fluid problems. *Rev. Geophys. Space Phys.*, **20**: 851–875.
- MESINGER, F. and ARAKAWA, A. 1976. Numerical Methods Used in Atmospheric Models, I. *Global Atmospheric Research Programme Publications Series, No. 17*, World Meteorological Organization, Geneva, 64 pp.
- PICKARD, G.L. 1975. Annual and longer term variations of deepwater properties of the coastal waters of Southern B.C. *J. Fish. Res. Board Can.* **32**: 1561–1587.
- SEMTNER, A.J. and CHERVIN, R.M. 1988. A simulation of the global ocean circulation with resolved eddies. *J. Geophys. Res.* **93**(C12): 15502–15522.
- SMAGORINSKY, J. 1963. General circulation experiments with the primitive equations. I. The basic experiment. *Mon. Weather Rev.* **91** (3): 99–164.
- SMITH, T.J. and TAKHAR, H.S. 1981. A mathematical model for partially mixed estuaries using the turbulence energy equation. *Estuar. Coastal Shelf Sci.* **13**: 27–45.
- STACEY, M.W. 1985. Some aspects of the internal tide in Knight Inlet, B.C., *J. Phys. Oceanogr.* **15**: 1652–1661.
- and POND, S. 1992. A numerical model of the internal tide in Knight Inlet, British Columbia. *ATMOSPHERE-OCEAN*, **30**(3): 383–418.
- ; ——— and NOWAK, Z.P. 1995. A numerical model of the circulation in Knight Inlet, British Columbia, Canada. *J. Phys. Oceanogr.* **25**: 1037–1062.
- and ———. 1997. On the Mellor-Yamada turbulence closure scheme: The surface boundary condition for  $q^2$ . *J. Phys. Oceanogr.* **27**: 2081–2086.
- WEBB, A.J. and POND, S. 1986a. A modal decomposition of the internal tide in a deep, strongly stratified inlet: Knight Inlet, British Columbia. *J. Geophys. Res.* **91** (C8): 9721–9738.
- and ———. 1986b. The propagation of a Kelvin wave around a bend in a channel. *J. Fluid Mech.* **169**: 257–274.
- YEREMY, M.L. 1995. A two-dimensional numerical model of Knight Inlet, British Columbia: Simulation of the temperature, salinity and velocity fields. M.Sc. thesis, Royal Roads Military College, Victoria, B.C., Canada, 131pp.
-